JCI The Journal of Clinical Investigation

NLRC4 suppresses melanoma tumor progression independently of inflammasome activation

Ann M. Janowski, … , Suzanne L. Cassel, Fayyaz S. Sutterwala

J Clin Invest. 2016;126(10):3917-3928. https://doi.org/10.1172/JCI86953.

Research Article **Immunology**

Members of the NLR family can assemble inflammasome complexes with the adaptor protein ASC and caspase-1 that result in the activation of caspase-1 and the release of IL-1β and IL-18. Although the NLRC4 inflammasome is known to have a protective role in tumorigenesis, there is an increased appreciation for the inflammasome-independent actions of NLRC4. Here, we utilized a syngeneic subcutaneous murine model of B16F10 melanoma to explore the role of NLRC4 in tumor suppression. We found that NLRC4-deficient mice exhibited enhanced tumor growth that was independent of the inflammasome components ASC and caspase-1. *Nlrc4* expression was critical for cytokine and chemokine production in tumor-associated macrophages and was necessary for the generation of protective IFN-γ–producing $CD4^+$ and $CD8^+$ T cells. Tumor progression was diminished when WT or caspase-1–deficient, but not NLRC4-deficient, macrophages were coinjected with B16F10 tumor cells in NLRC4-deficient mice. Finally, examination of human primary melanomas revealed the extensive presence of $NLRC4^+$ tumor-associated macrophages. In contrast, there was a paucity of $NLRC4^+$ tumor-associated macrophages observed in human metastatic melanoma, supporting the concept that NLRC4 expression controls tumor growth. These results reveal a critical role for NLRC4 in suppressing tumor growth in an inflammasome-independent manner.

NLRC4 suppresses melanoma tumor progression independently of inflammasome activation

Ann M. Janowski,[1,2] Oscar R. Colegio,[3] Emma E. Hornick,[1,2] Jennifer M. McNiff,[3] Matthew D. Martin,[2,4] Vladimir P. Badovinac,[2,4] Lyse A. Norian,[5] Weizhou Zhang,[2,4] Suzanne L. Cassel,[1,2,6,7] and Fayyaz S. Sutterwala[1,2,6,7]

[1]Inflammation Program and [2]Interdisciplinary Program in Immunology, University of Iowa, Iowa City, Iowa, USA. [3]Department of Dermatology, Yale University School of Medicine, New Haven, Connecticut, USA. [4]Department of Pathology, University of Iowa, Iowa City, Iowa, USA. [5]Department of Nutrition Sciences, University of Alabama at Birmingham, Birmingham, Alabama, USA. [6]Department of Internal Medicine, University of Iowa, Iowa City, Iowa, USA. [7]Department of Medicine, Cedars-Sinai Medical Center, Los Angeles, California, USA.

Members of the NLR family can assemble inflammasome complexes with the adaptor protein ASC and caspase-1 that result in the activation of caspase-1 and the release of IL-1β and IL-18. Although the NLRC4 inflammasome is known to have a protective role in tumorigenesis, there is an increased appreciation for the inflammasome-independent actions of NLRC4. Here, we utilized a syngeneic subcutaneous murine model of B16F10 melanoma to explore the role of NLRC4 in tumor suppression. We found that NLRC4-deficient mice exhibited enhanced tumor growth that was independent of the inflammasome components ASC and caspase-1. *Nlrc4* expression was critical for cytokine and chemokine production in tumor-associated macrophages and was necessary for the generation of protective IFN-γ–producing CD4$^+$ and CD8$^+$ T cells. Tumor progression was diminished when WT or caspase-1–deficient, but not NLRC4-deficient, macrophages were coinjected with B16F10 tumor cells in NLRC4-deficient mice. Finally, examination of human primary melanomas revealed the extensive presence of NLRC4$^+$ tumor-associated macrophages. In contrast, there was a paucity of NLRC4$^+$ tumor-associated macrophages observed in human metastatic melanoma, supporting the concept that NLRC4 expression controls tumor growth. These results reveal a critical role for NLRC4 in suppressing tumor growth in an inflammasome-independent manner.

Introduction

Melanoma is one of the deadliest forms of skin cancer, and advanced cases of melanoma are especially hard to treat due to limited therapeutic options (1, 2). Increased risk of melanoma is associated with UV-induced mutations, inflammation, genetic predisposition, and other causes (3–5). Inflammation in the tumor microenvironment is driven by many factors, including the presence of the proinflammatory cytokine IL-1β (6–8). A major source of IL-1β secretion occurs through the activation of inflammasomes. Inflammasomes are multiprotein complexes that, upon activation, trigger the autocatalytic cleavage of the cysteine protease caspase-1 (9, 10). Caspase-1 then cleaves pro–IL-β and pro–IL-18 into their mature secreted forms. Currently there are at least 4 defined inflammasomes: NLRP1, NLRP3, NLRC4, and AIM2 (9, 10).

The NLRC4 inflammasome is composed of NLRC4, the adaptor protein ASC, and caspase-1 (11, 12). Known activators of the NLRC4 inflammasome include Gram-negative bacteria such as *Salmonella typhimurium* (13), *Pseudomonas aeruginosa* (14, 15), *Klebsiella pneumonia* (16), and *Legionella pneumophila* (17, 18). More specifically, neuronal apoptosis inhibitor proteins (NAIP) recognize flagellin (NAIP5 and NAIP6), type III secretion system (T3SS) rod protein (NAIP2), and the T3SS needle protein (NAIP1) from Gram-negative bacteria, leading to activation of the NLRC4 inflammasome (19–26). In addition to the recognition and control of bacterial pathogens, the NLRC4 inflammasome plays a protective role in tumorigenesis in an azoxymethane and dextran sodium sulfate colitis-associated colorectal cancer model (27). Both NLRC4- and caspase-1–deficient mice exhibited increased tumor burdens compared with WT mice (27). However, the role of NLRC4 in the development and progression of other malignancies, and in particular melanoma, is completely unknown. Importantly, a function for NLRC4 independent of an inflammasome and caspase-1 has never been described.

In this study, we demonstrate a protective role for NLRC4 in a s.c. B16F10 melanoma model. Unexpectedly, mice deficient in the inflammasome components ASC and caspase-1 had tumors the same size as WT mice, suggesting that regulation of tumor growth is dependent on NLRC4, but independent of NLRC4 inflammasome activation. Examination of the tumor microenvironment showed a decrease in IFN-γ–positive tumor-infiltrating CD4$^+$ and CD8$^+$ T cells and a global alteration of the cytokine and chemokine milieu in *Nlrc4*$^{-/-}$ mice. The addition of WT or caspase-1–deficent, but not NLRC4-deficient, macrophages into *Nlrc4*$^{-/-}$ mice at the time of tumor challenge led to decreased tumor growth compared with challenge with B16F10 tumors alone. Importantly, we observed substantial numbers of NLRC4$^+$ tumor-associated macrophages in primary human melanomas, but not in more advanced metastatic disease. Together, our findings demonstrate an inflammasome-independent role for NLRC4 expression in macrophages, which is required to generate the immune response necessary for suppression of melanoma progression.

Authorship note: S.L. Cassel and F.S. Sutterwala contributed equally to this work.
Conflict of interest: The authors have declared that no conflict of interest exists.
Submitted: February 5, 2016; **Accepted:** August 2, 2016.
Reference information: *J Clin Invest*. 2016;126(10):3917–3928. doi:10.1172/JCI86953.

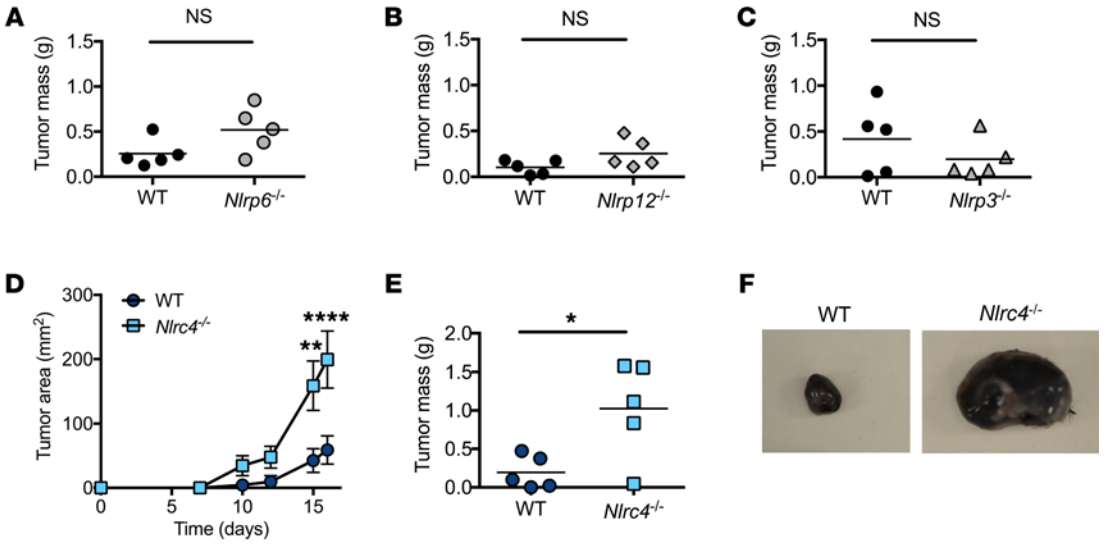

Figure 1. NLRC4 protects against B16F10 tumor growth in vivo. (**A**–**F**) WT and *Nlrp6*$^{-/-}$ (**A**), *Nlrp12*$^{-/-}$ (**B**), *Nlrp3*$^{-/-}$ (**C**), and *Nlrc4*$^{-/-}$ (**D**–**F**) mice were injected s.c. with 1×10^5 B16F10 cells. (**A**–**C** and **E**) Tumor mass was determined at 16 to 20 days after inoculation. (**D**) WT and *Nlrc4*$^{-/-}$ tumor areas (length × width) were measured every 2 to 3 days. (**F**) Representative images of excised WT and *Nlrc4*$^{-/-}$ B16F10 tumors. (**A**–**E**) Data are representative of 3 independent experiments with $n = 5$ mice per group. (**A**–**C** and **E**) $^*P \le 0.05$, unpaired 2-tailed Student's t test. (**D**) Error bars represent SEM. $^{**}P \le 0.01$, $^{****}P \le 0.0001$, 2-way ANOVA with Šidák's multiple comparisons test.

Results

NLRC4 is critical for control of s.c. tumor growth. To determine whether members of the NLR family of proteins regulate growth of s.c. tumors, we challenged *Nlrp6*$^{-/-}$, *Nlrp12*$^{-/-}$, and *Nlrp3*$^{-/-}$ mice with B16F10 melanoma cells s.c. Neither *Nlrp6*$^{-/-}$, *Nlrp12*$^{-/-}$, nor *Nlrp3*$^{-/-}$ mice had altered tumor size compared with WT mice (Figure 1, A–C), indicating that NLRP6, NLRP12, and NLRP3 were dispensable for the control of s.c. B16F10 tumor growth. In contrast, NLRC4-deficient mice exhibited a marked increase in tumor size in comparison with WT mice following s.c. challenge with B16F10 cells (Figure 1, D–F).

We next sought to determine whether expression of NLRC4 was necessary for regulation of different types of s.c. tumors or whether the protective role of NLRC4 was specific to B16F10 melanoma. To address this question, we challenged *Nlrc4*$^{-/-}$ and WT mice s.c. with Lewis lung carcinoma (LLC) cells. As seen with the B16F10 model, *Nlrc4*$^{-/-}$ mice had markedly increased tumor size and mass compared with WT mice when challenged s.c. with LLC cells (Supplemental Figure 1, A–C; supplemental material available online with this article; doi:10.1172/JCI86953DS1). These data demonstrate a previously undescribed role for NLRC4 in suppressing s.c. tumor growth in 2 tumor models.

Diminished NLRC4$^+$ *tumor-associated macrophages in human metastatic melanoma*. To determine whether NLRC4 was present in human primary melanoma, we performed immunohistochemistry on normal skin, benign melanocytic nevi, primary invasive melanoma, and metastatic melanoma from human patients using the macrophage marker CD163 and NLRC4. Both normal skin and benign melanocytic nevi displayed a minimal presence of CD163$^+$ macrophages and NLRC4$^+$ cells (Figure 2, A and B). In contrast, primary invasive melanoma had a significantly greater density of NLRC4$^+$ cells, which were determined to be tumor-associated macrophages by dually staining the melanomas for CD163 and NLRC4 (Figure 2, A and B, and Supplemental Figure 2). Examination of human metastatic melanoma also revealed a high density of CD163$^+$ tumor-associated macrophages. Surprisingly, macrophages present in metastatic melanoma did not express significant amounts of NLRC4 (Figure 2, A and B).

NLRC4 acts independently of the inflammasome to modulate s.c. tumor growth. In conjunction with ASC and caspase-1, NLRC4 forms an inflammasome complex that results in the activation of caspase-1 (12). To date, no inflammasome-independent functions of NLRC4 have been described. To determine whether NLRC4 inflammasome activation was critical for protection during tumor challenge, we challenged *Asc*$^{-/-}$ and *Casp1*$^{-/-}$ mice s.c. with B16F10 cells. Unexpectedly, *Asc*$^{-/-}$ and *Casp1*$^{-/-}$ mice had tumor mass and area that were the same as the tumors from WT mice (Figure 3, A–D), indicating that the inflammasome was not necessary for tumor suppression. These results were also confirmed using the LLC s.c. model where both *Asc*$^{-/-}$ mice (Supplemental Figure 1, D and E) and *Casp1*$^{-/-}$ mice (Supplemental Figure 1, F and G) exhibited tumor growth similar to that of WT mice after LLC challenge.

Consistent with these data, we observed intact caspase-1 activation in B16F10 tumors isolated from *Nlrc4*$^{-/-}$ mice as detected by the presence of the p20 cleavage product of caspase-1 by immunoblot (Figure 3E). Taken together, these data suggest that NLRC4-mediated protection against tumor growth is independent of an inflammasome.

Expression of NLRC4 in hematopoietic cells is important for controlling tumor growth. NLRC4 is expressed in a variety of cells, including macrophages, dendritic cells, fibroblasts, and intestinal epithelial cells, among others (28). A wide array of myeloid and lymphoid cell types infiltrate solid tumors and affect tumor growth (29). Additionally, there are also stromal cells that reside in the tumor, such as cancer-associated fibroblasts, that also modulate tumor growth and angiogenesis (30). Consistent with previous studies, we found high expression of *Nlrc4* in macrophages

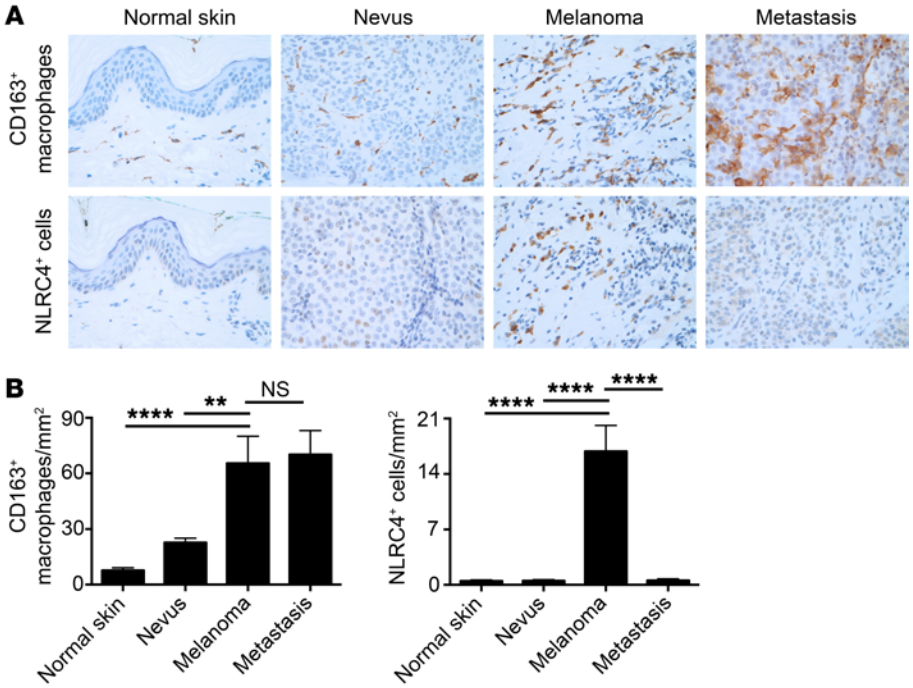

Figure 2. Human primary melanoma is enriched with NLRC4$^+$ macrophages. (**A**) Deidentified skin biopsies of normal skin (n = 3 patients), benign melanocytic nevi (n = 3 patients), primary invasive melanomas (n = 3 patients), and metastatic melanomas (n = 3 patients) were stained for CD163 (brown) and NLRC4 (brown). Images were taken with a ×40 objective. (**B**) The densities of five 20× high-power fields (each 3.14 mm^2) were determined per patient sample. $^{**}P \le 0.01$; $^{****}P \le 0.0001$, Mann–Whitney U test.

with lower expression in fibroblasts and CD4$^+$ and CD8$^+$ T cells (Figure 4A), demonstrating that NLRC4 is expressed in cell types known to affect tumor growth. Importantly, there was no detectable expression of *Nlrc4* within B16F10 or LLC cells, indicating that NLRC4 in the tumor cells themselves is unlikely to be modulating tumor growth (Figure 4A).

As *Nlrc4* was expressed in both the hematopoietic and nonhematopoietic compartments, we next asked in which compartment NLRC4 acted to regulate tumor growth through the generation of BM chimeric mice. As expected, WT mice reconstituted with WT BM (WT donor → WT recipient) had significantly smaller tumor mass and area than *Nlrc4*$^{-/-}$ mice reconstituted with *Nlrc4*$^{-/-}$ BM (*Nlrc4*$^{-/-}$ donor → *Nlrc4*$^{-/-}$ recipient) consistent with NLRC4 playing a protective role in B16F10 tumor progression (Figure 4, B and C). *Nlrc4*$^{-/-}$ mice reconstituted with WT BM (WT donor → *Nlrc4*$^{-/-}$ recipient) exhibited a similar tumor mass and area compared with WT control mice (WT donor → WT recipient) (Figure 4, B and C), indicating that the addition of WT BM into an *Nlrc4*$^{-/-}$ mouse is sufficient to suppress B16F10 tumor growth. In contrast, WT mice reconstituted with *Nlrc4*$^{-/-}$ BM (*Nlrc4*$^{-/-}$ donor → WT recipient) displayed a significant increase in tumor size compared with *Nlrc4*$^{-/-}$ mice reconstituted with WT BM (WT donor → *Nlrc4*$^{-/-}$ recipient) (Figure 4, B and C).

We also observed that WT mice reconstituted with *Nlrc4*$^{-/-}$ BM (*Nlrc4*$^{-/-}$ donor → WT recipient) had smaller tumors compared with *Nlrc4*$^{-/-}$ control mice (*Nlrc4*$^{-/-}$ donor → *Nlrc4*$^{-/-}$ recipient) (Figure 4, B and C). This suggests that the nonhematopoietic compartment may be playing a role in modulating tumor growth or that there may be a synergistic role between *Nlrc4*$^{-/-}$ hematopoietic and nonhematopoietic cells that leads to enhanced tumor growth. It may also be reasoned that WT hematopoietic cells that are radio resistant remained in the skin after irradiation and subsequent reconstitution with *Nlrc4*$^{-/-}$ BM. The presence of WT radio-resistant cells may also result in a decrease in tumor size in WT mice reconstituted with *Nlrc4*$^{-/-}$ BM compared with *Nlrc4*$^{-/-}$ control mice. Taken together, these data suggest that expression of NLRC4 in a hematopoietic cell is important for controlling tumor growth along with a possible contribution of NLRC4 from the nonhematopoietic compartment.

Macrophage Nlrc4 expression modulates tumor cytokine and chemokine levels. Within the tumor microenvironment, there is an intricate network of cytokines and chemokines that affects tumor-infiltrating cells and alters the function of cells already present in the tumor (31, 32). To determine whether the cytokine and chemokine milieu was different between tumors from WT and *Nlrc4*$^{-/-}$ mice, we utilized a quantitative PCR (qPCR) profile array that examines 84 different cytokines and chemokines. We observed a marked decrease in gene expression of a wide array of cytokines and chemokines in tumors from *Nlrc4*$^{-/-}$ mice compared with WT (Figure 5, A–F, and Supplemental Table 1). Of particular interest was the decrease in *Cxcl9*, *Cxcl10*, *Cxcl16*, and *Ccl5* expression in tumors from *Nlrc4*$^{-/-}$ mice, as these chemokines have been implicated as pivotal in the recruitment of effector T cells to the tumor (33–35).

We next sought to determine which cell type was responsible for the altered cytokine and chemokine production in the tumors from *Nlrc4*$^{-/-}$ mice. Since NLRC4 is highly expressed in macrophages (Figure 4A) and in particular in tumor-associated macro-

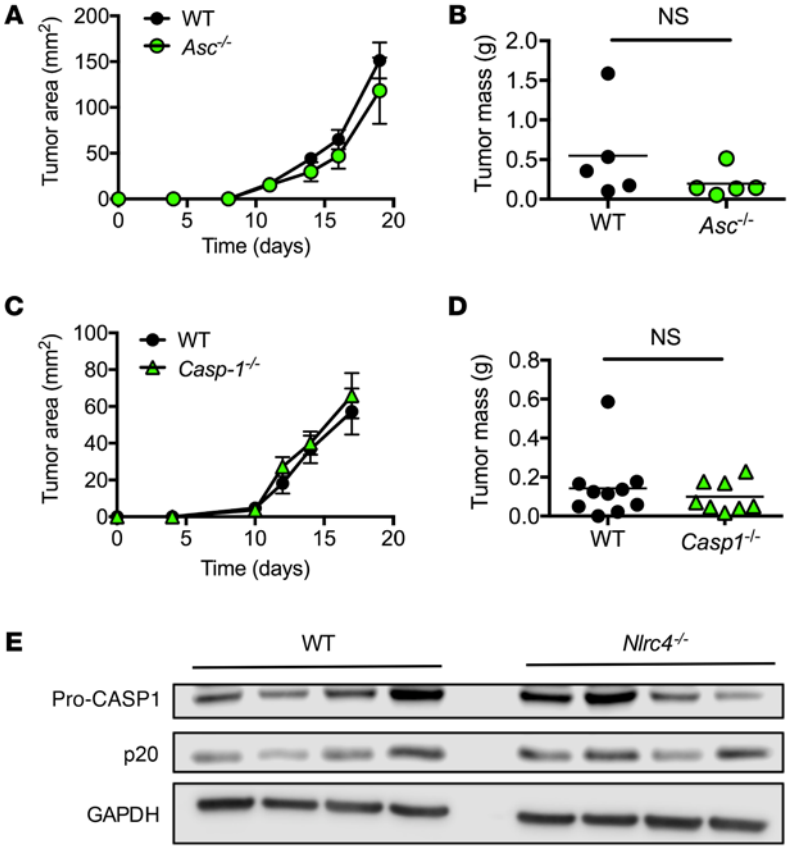

Figure 3. NLRC4-mediated protection against tumor growth is independent of inflammasome activation. (**A**–**D**) WT, *Asc*$^{-/-}$ (**A** and **B**), and *Casp1*$^{-/-}$ (**C** and **D**) mice were injected s.c. with 1×10^5 B16F10 cells. (**A** and **C**) Tumor area was measured every 2 to 3 days. (**B** and **D**) Tumor mass was determined at 17 to 20 days after inoculation. (**A**–**D**) Data are representative of 3 experiments with $n \geq 5$ mice per group. (**A** and **C**) Error bars represent SEM. (**B** and **D**) Unpaired 2-tailed Student's *t* test. (**E**) B16F10 tumors from WT and *Nlrc4*$^{-/-}$ mice on day 14 after inoculation were homogenized and immunoblotted with antibodies against caspase-1 and GAPDH. Each lane represents a tumor from an individual mouse. Data are representative of 2 independent experiments.

phages in primary human melanomas (Figure 2, A and B), we sorted F4/80$^+$CD45.2$^+$ macrophages and CD45.2$^-$ nonhematopoietic cells from B16F10 tumors from WT and *Nlrc4*$^{-/-}$ mice. After sorting, we examined expression of chemokines that were markedly decreased in tumors from *Nlrc4*$^{-/-}$ mice: *Cxcl9*, *Cxcl10*, *Cxcl13*, and *Cxcl16*. Expression of these chemokines was reduced in tumor-infiltrating F4/80$^+$CD45.2$^+$ macrophages from *Nlrc4*$^{-/-}$ mice compared with those from WT (Figure 5G). However, there was no difference in expression of these chemokines in CD45.2$^-$ cells from *Nlrc4*$^{-/-}$ and WT mice (Figure 5H). Thus, the decreased expression of chemokines in tumors from *Nlrc4*$^{-/-}$ mice appeared to be due to decreased expression of these chemokines in tumor-associated macrophages.

Consistent with our findings suggesting NLRC4 deficient macrophages are responsible for the impaired chemokine production in tumors in *Nlrc4*$^{-/-}$ mice, BM-derived macrophages (BMDMs) from *Nlrc4*$^{-/-}$ mice challenged with B16F10 whole-tumor homogenate in vitro had reduced chemokine expression compared with WT BMDMs (Figure 5I). BMDMs from *Nlrc4*$^{-/-}$ mice also produced diminished IL-6 and IL-12p40 in response to stimulation with TLR2 and TLR4 agonists (Figure 5, J and K). In contrast, *Asc*$^{-/-}$ and *Casp1*$^{-/-}$ BMDMs had intact IL-6 and IL-12p40 production in response to TLR agonists (Supplemental Figure 3, A and B). Taken together, these data suggest that NLRC4 plays a role in cytokine and chemokine production in response to multiple stimuli in an inflammasome-independent manner.

Tumor-associated macrophages produce increased levels of suppressive cytokines and decreased levels of proinflammatory cytokines, including IL-12 (36). Tumor-associated macrophages are also characterized by a specific transcriptional profile, including expression of the genes arginase 1 (*Arg1*), found in inflammatory zone (*Fizz1*), and macrophage protein (*Ym1*) (37, 38). Due to the decreased production of IL-12p40 by NLRC4-deficient BMDMs in response to classic proinflammatory stimulus and the larger tumor size in *Nlrc4*$^{-/-}$ mice, we examined the expression of *Arg1*, *Fizz1*, and *Ym1* in tumors from WT and *Nlrc4*$^{-/-}$ mice. Surprisingly, we did not observe any difference in *Arg1* and *Fizz1* gene expression in tumors from WT and *Nlrc4*$^{-/-}$ mice (Supplemental Figure 4, A and B). However, we did observe a small increase in *Ym1* expression in tumors from *Nlrc4*$^{-/-}$ mice (Supplemental Figure 4C). We also examined gene expression in F4/80$^+$CD45.2$^+$ macrophages isolated from tumors from WT and *Nlrc4*$^{-/-}$ mice and observed no significant differences in *Arg1*, *Fizz1*, and *Ym1* expression (Supplemental Figure 4, D and E).

NLRC4 regulates STAT3 signaling in vivo and in vitro. Other NLRs, such as NLRP6 and NLRP12, have been established as regulators of signaling pathways, such as canonical and noncanonical NF-κB and MAPK pathways (39–42). Furthermore, the decreased expression of cytokines and chemokines points to a defect in proinflammatory signaling pathways. To determine whether NLRC4 was capable of regulating these pathways in the tumor microenvironment, we took whole B16F10 tumor homogenates from WT and *Nlrc4*$^{-/-}$ mice and examined activation of various signaling pathways via immunoblotting. Tumors from *Nlrc4*$^{-/-}$ mice exhibited a decrease in STAT3 phosphorylation (Figure 6A) and an increase in p38 phosphorylation (Figure 6B). No difference in activation of ERK or JNK pathways (Supplemental Figure 5, A and B) was observed. Additionally, no detectable difference in phosphorylation of IκBα or degradation of p100 into p52 was observed, suggesting that canonical and noncanonical NF-κB pathways were intact in *Nlrc4*$^{-/-}$ mice (Supplemental Figure 5, C and D).

In addition, we examined phosphorylation of STAT3 and p38 in vitro in WT and *Nlrc4*$^{-/-}$ BMDMs in response to stimulation with LPS. In line with the in vivo data, we observed a decrease in STAT3 phosphorylation in *Nlrc4*$^{-/-}$ BMDMs compared with WT BMDMs at 6 and 7 hours after stimulation (Figure 6C). We only observed a modest increase in phosphorylation of p38 in *Nlrc4*$^{-/-}$ BMDMs at 60 minutes after LPS challenge (Figure 6D). Therefore, it is likely that the increase in p38 phosphorylation in the tumors from *Nlrc4*$^{-/-}$ mice is due to a cell population other than macrophages.

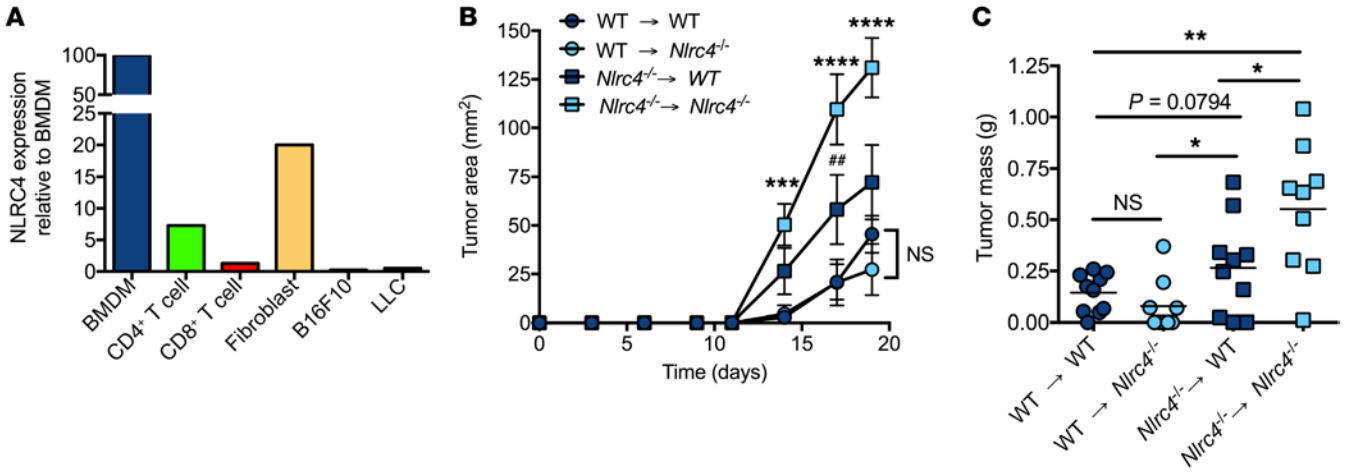

Figure 4. Expression of *Nlrc4* in hematopoietic cells is important for controlling tumor growth. (**A**) Expression of *Nlrc4* in BMDMs, fibroblasts, CD4$^+$ T cells, CD8$^+$ T cells, B16F10, and LLC cells was determined by qPCR and represented as expression relative to *Nlrc4* expression in BMDMs. Data are representative of 2 independent experiments. (**B** and **C**) WT and *Nlrc4*$^{-/-}$ mice were lethally irradiated and reconstituted with either WT or *Nlrc4*$^{-/-}$ BM (donor BM → recipient mouse). Mice were injected s.c. with 1 × 10^5 B16F10 cells. (**B**) Tumor area was measured every 2 to 3 days. (**C**) Tumor mass was determined at day 19 after inoculation. (**B** and **C**) Data are representative of 2 experiments with $n \geq 9$ mice per experiment. (**B**) Error bars represent SEM. $^{\#\#}P \leq 0.01$ (for *Nlrc4*$^{-/-}$ → WT compared with WT → WT); $^{***}P \leq 0.001$ and $^{****}P \leq 0.0001$ (for *Nlrc4*$^{-/-}$ → *Nlrc4*$^{-/-}$ compared with WT → WT), 2-way ANOVA with Tukey's HSD post-test for multiple comparisons. (**C**) $^{*}P \leq 0.05$, $^{**}P \leq 0.01$, unpaired 2-tailed Student's *t* test.

Stimulation of *Nlrc4*$^{-/-}$ BMDMs with LPS resulted in decreased production of the cytokine IL-6 compared with WT (Figure 5J). Since IL-6 is a known activator of the STAT3 signaling pathway (43), it was important to address whether there was an intrinsic defect in STAT3 signaling in *Nlrc4*$^{-/-}$ BMDMs or whether the decrease in IL-6 production was subsequently leading to decreased STAT3 activation in these cells. We challenged both WT and *Nlrc4*$^{-/-}$ BMDMs with recombinant IL-6 and observed no notable differences in STAT3 phosphorylation (Figure 6E), suggesting that the decrease in STAT3 activation in vitro is due to decreased IL-6 production by *Nlrc4*$^{-/-}$ macrophages.

We also examined activation of ERK, JNK, and canonical and noncanonical NF-κB pathways in vitro. In response to stimulation with LPS, we observed no differences in phosphorylation of ERK and JNK (Supplemental Figure 6, A and B) in WT and *Nlrc4*$^{-/-}$ BMDMs. In contrast to in vivo data, we observed a modest decrease in phosphorylation of IκBα in *Nlrc4*$^{-/-}$ BMDMs compared with WT (Supplemental Figure 6C). We next examined activation of the noncanonical NF-κB pathway in response to TNF-α and anti-CD40 antibody in vitro; we observed no difference in activation to either stimulus in WT and *Nlrc4*$^{-/-}$ BMDMs (Supplemental Figure 6D).

NLRC4-deficient mice have defective IFN-γ production in the tumor microenvironment. CD4$^+$ Th1 and CD8$^+$ T cells represent a crucial part of the antitumor immune response. In addition, IFN-γ is a key cytokine produced by T cells that is critical in controlling tumor growth (44). Chemokines such as CXCL9, CXCL10, CXCL16, and CCL5 play an important role in recruiting effector T cells into the tumor (33–35); importantly, expression of these chemokines was markedly diminished in tumors in *Nlrc4*$^{-/-}$ mice (Figure 5, A–F). To determine whether this defective production of cytokines and chemokines affected the composition of infiltrating immune cells in the tumors of *Nlrc4*$^{-/-}$ mice, we looked at the cellular makeup of hematopoietic cells within the tumors utilizing flow cytometry. The frequency of total CD4$^+$ and CD8$^+$ T cells within the tumors of WT and *Nlrc4*$^{-/-}$ mice was similar (Figure 7, A and B). However, there were significantly decreased frequencies of IFN-γ–producing CD4$^+$ and CD8$^+$ T cells in the tumors of *Nlrc4*$^{-/-}$ mice (Figure 7, C and D). This decrease in IFN-γ production in *Nlrc4*$^{-/-}$ mice was also confirmed by examining IFN-γ gene expression in the whole tumor via qPCR (Figure 7E). We did not observe differences in production of other effector cytokines and molecules such as TNF-α and granzyme B by T cells (data not shown). These data demonstrate an impaired effector CD4$^+$ Th1 and CD8$^+$ T cell response in the tumors of *Nlrc4*$^{-/-}$ mice that could explain the enhanced tumor growth in these animals.

To determine whether the defect in IFN-γ–producing CD4$^+$ and CD8$^+$ T cells was restricted to tumor-infiltrating T cells, we examined the T cell composition of tumor-draining lymph nodes from WT and *Nlrc4*$^{-/-}$ mice. We observed no differences in overall frequency of CD4$^+$ T cells and CD8$^+$ T cells in the lymph nodes of WT and *Nlrc4*$^{-/-}$ mice (Supplemental Figure 7, A and B). Importantly both CD4$^+$ and CD8$^+$ T cells from the lymph nodes of WT and *Nlrc4*$^{-/-}$ mice produced similar levels of IFN-γ following PMA/ionomycin stimulation (Supplemental Figure 7, C and D). These data suggest that T cells from *Nlrc4*$^{-/-}$ mice do not have an intrinsic defect or are improperly primed in the lymph node. Hence, it is a possibility that tumor-infiltrating effector CD4$^+$ and CD8$^+$ T cells in *Nlrc4*$^{-/-}$ mice are being suppressed in the tumor microenvironment and therefore producing less IFN-γ. It is also possible that there is a defect in migration of effector T cells into the tumor in *Nlrc4*$^{-/-}$ mice.

We sought to further characterize the composition of infiltrating cells in the tumor microenvironment of WT and *Nlrc4*$^{-/-}$ mice. We observed no difference in the frequency of F4/80$^+$ macrophages, CD11c$^+$MHCII$^+$ dendritic cells, CD11b$^+$GR1$^+$ monocytic cells (myeloid-derived suppressor cells), and Foxp3$^+$CD4$^+$

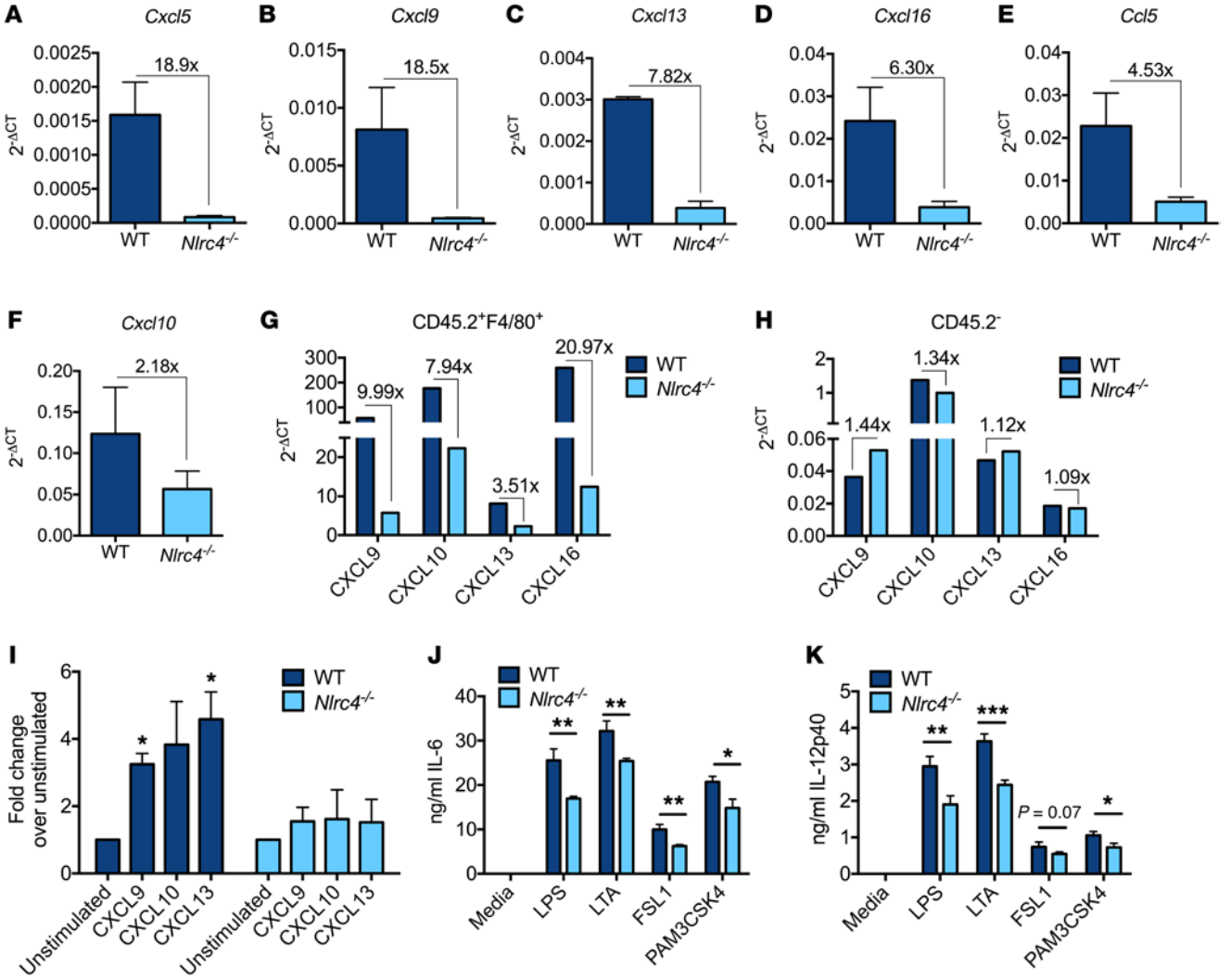

Figure 5. Absence of NLRC4 in macrophages alters the tumor cytokine and chemokine milieu. (**A**–**F**) WT and *Nlrc4*$^{-/-}$ mice were injected s.c. with 1 × 10^5 B16F10 cells. On day 12 after inoculation, total RNA was isolated from homogenized tumors and used to determine cytokine and chemokine expression via quantitative qPCR utilizing a PCR array. Selected genes from the array are displayed; data are pooled from 3 separate experiments (n = 3 mice per group). (**G** and **H**) WT and *Nlrc4*$^{-/-}$ mice were injected s.c. with 1 × 10^5 B16F10 cells; 14 days after inoculation, tumors were harvested, pooled, and FACS sorted based on CD45.2 and F4/80 staining. RNA was isolated from CD45.2$^-$ and CD45.2$^+$F4/80$^+$ cells and used to determine *Cxcl9*, *Cxcl10*, *Cxcl13*, and *Cxcl16* expression by qPCR; data are representative of 2 independent experiments with $n \geq 5$ pooled tumors per group. (**I**) WT and *Nlrc4*$^{-/-}$ BMDMs were challenged for 9 hours with B16F10 whole tumor homogenate. *Cxcl9*, *Cxcl10*, and *Cxcl13* expression was determined by qPCR. Data are pooled from 3 independent experiments, and fold change in gene expression is relative to unstimulated samples. (**J** and **K**) WT and *Nlrc4*$^{-/-}$ BMDMs were challenged with 50 ng/ml LPS, 50 μg/ml LTA, 100 ng/ml FSL-1, and 1 μg/ml Pam3CSK4. Twenty hours later, supernatants were collected and levels of IL-6 (**J**) and IL-12p40 (**K**) determined by ELISA; data are representative of 3 independent experiments. (**A**–**F** and **I**) Error bars represent SEM. (**J** and **K**) Error bars represent SD. (**I**–**K**) *$P \leq 0.05$, **$P \leq 0.01$, and ***$P \leq 0.001$, unpaired 2-tailed Student's t test.

Treg cells between tumors from WT and *Nlrc4*$^{-/-}$ mice (Figure 7, F–I). However, it remains possible that, although there were no observed differences in frequencies in these cell types, they may be functionally defective. Together, these data suggest the failure to contain tumor growth in *Nlrc4*$^{-/-}$ mice may be due in part to the inability of effector CD4$^+$ and CD8$^+$ T cells to produce IFN-γ. Because NLRC4 is not highly expressed in T cells (Figure 4A), it is likely that NLRC4 is acting in another cell type, such as a macrophage, to suppress tumor growth and enhance T cell function.

NLRC4 expression in macrophages is critical for controlling tumor growth. Our findings support the hypothesis that macrophages deficient in NLRC4 are less inflammatory than WT macrophages and that this results in either a failure of appropriate recruitment of adaptive immune cells or suppression of immune cells in the tumor microenvironment. To assess whether defective macrophage function in *Nlrc4*$^{-/-}$ mice was responsible for enhanced tumor growth, we challenged *Nlrc4*$^{-/-}$ mice s.c. with B16F10 cells alone or B16F10 cells with WT or *Nlrc4*$^{-/-}$ BMDMs. *Nlrc4*$^{-/-}$ mice challenged with B16F10 cells and *Nlrc4*$^{-/-}$ BMDMs developed tumor area and mass similar to that of mice challenged with only B16F10 cells (Figure 8, A and B). Importantly, when *Nlrc4*$^{-/-}$ mice were challenged with B16F10 cells in the presence of WT BMDMs, the resultant tumors were smaller than in mice that received NLRC4-deficient macrophages or tumor cells

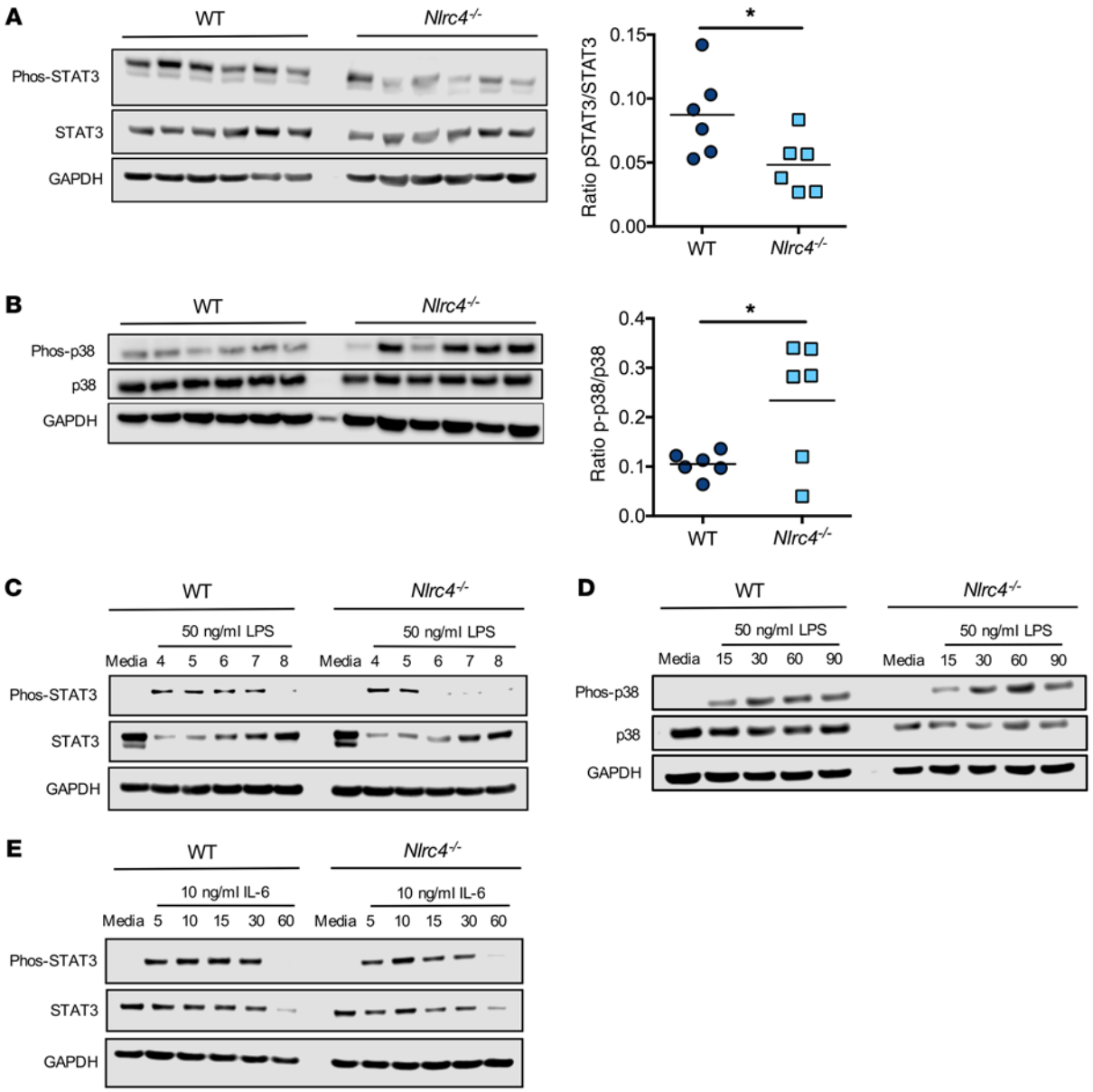

Figure 6. NLRC4 regulates STAT3 and p38 MAPK signaling in the tumor microenvironment. (**A** and **B**) B16F10 tumors from WT and *Nlrc4*$^{-/-}$ mice at day 14 after inoculation were homogenized and immunoblotted for phospho-STAT3 and STAT3 (**A**), phospho-p38 MAPK and p38 MAPK (**B**), and GAPDH (**A** and **B**). Each lane represents a tumor from an individual mouse. (**A** and **B**) Densitometry of the ratio of phosphorylated to total protein is shown. (**C**) WT and *Nlrc4*$^{-/-}$ BMDMs were challenged for 4, 5, 6, 7, and 8 hours with 50 ng/ml LPS. Cell lysates were immunoblotted with antibodies against phospho-STAT3, STAT3, and GAPDH. (**D**) WT and *Nlrc4*$^{-/-}$ BMDMs were challenged for 15, 30, 60, and 90 minutes with 50 ng/ml LPS. Cell lysates were immunoblotted with antibodies against phospho-p38 MAPK, p38 MAPK, and GAPDH. (**E**) WT and *Nlrc4*$^{-/-}$ BMDMs were challenged for 5, 10, 15, 30, and 60 minutes with 10 ng/ml recombinant IL-6. Cell lysates were immunoblotted with antibodies against phospho-STAT3, STAT3, and GAPDH. (**C–E**) Data are representative of 3 independent experiments. (**A** and **B**) $^*P \leq 0.05$, unpaired 2-tailed Student's *t* test.

alone (Figure 8, A and B). These data support the results seen in the BM chimera experiments (Figure 4, B and C) and further indicate that expression of NLRC4 in macrophages is required for controlling tumor growth.

We found that control of B16F10 tumor growth was dependent on NLRC4, but independent of the inflammasome components ASC and caspase-1 (Figure 3). In order to determine whether suppression of tumor growth by macrophages was also inflammasome independent, we injected *Nlrc4*$^{-/-}$ mice s.c. with B16F10 cells alone or B16F10 cells with *Casp1*$^{-/-}$ BMDMs. The addition of *Casp1*$^{-/-}$ BMDMs reduced B16F10 tumor area and mass (Figure 8, C and D), thus demonstrating that NLRC4, and not inflammasome activation, in macrophages is required to control tumor growth.

Discussion

Our work demonstrates that NLRC4, in an inflammasome-independent manner, plays an essential role in suppressing melanoma progression. There is an increasing appreciation for the role of NLRs and

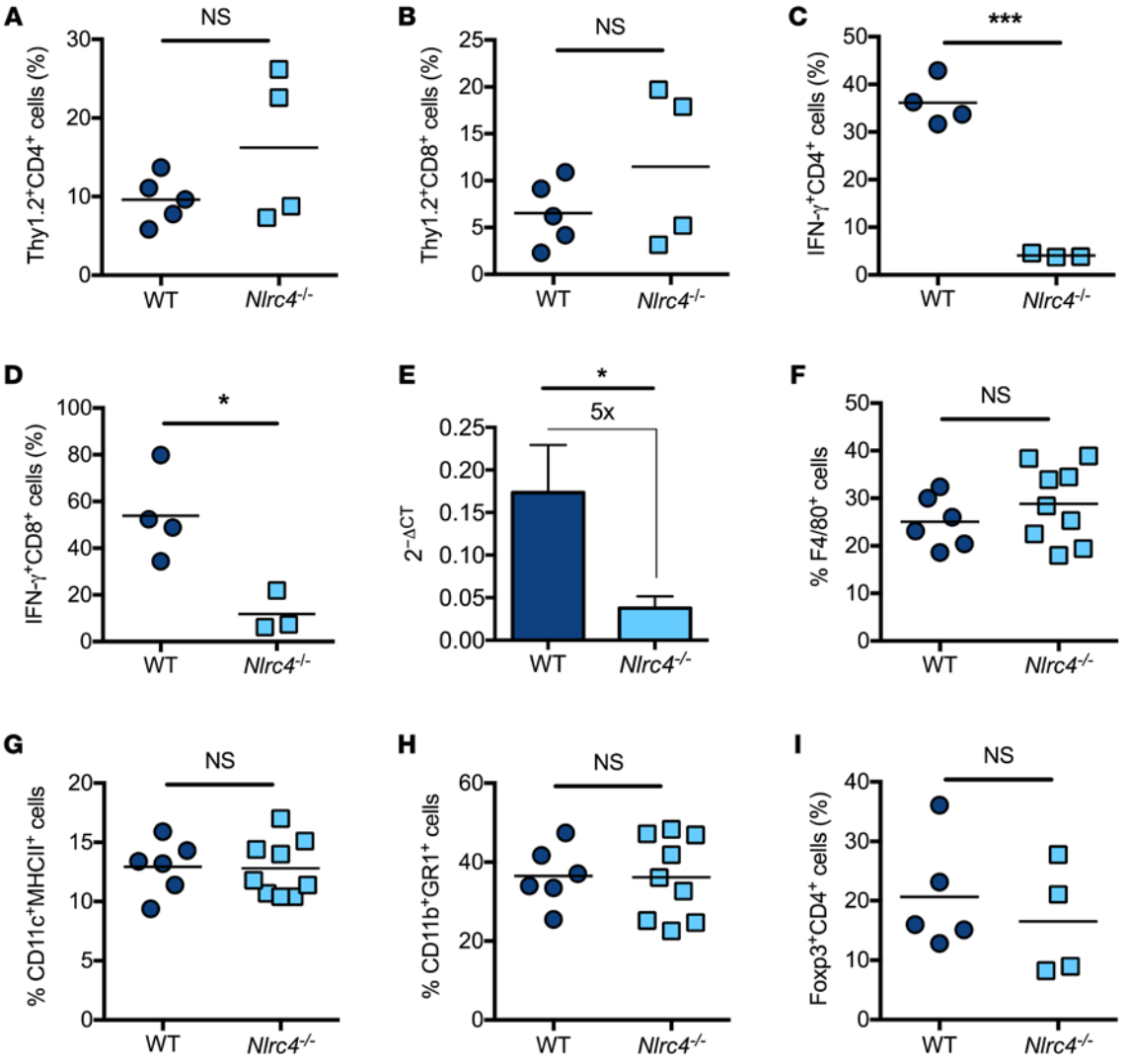

Figure 7. NLRC4 is required for IFN-γ⁺ tumor-infiltrating effector CD4⁺ and CD8⁺ T cells. (**A**–**I**) WT and *Nlrc4*$^{-/-}$ mice were injected s.c. with 1 × 10^5 B16F10 cells. (**A**–**D** and **F**–**I**) On day 14 after inoculation, tumors were made into single-cell suspensions for flow cytometry; the CD45.2⁺ population was gated on and the frequency of Thy1.2⁺CD4⁺ T cells (**A**), Thy1.2⁺CD8⁺ T cells (**B**), F4/80⁺ macrophages (**F**), CD11c⁺MHCII⁺ dendritic cells (**G**), CD11b⁺GR1⁺ monocytes (**H**), and Foxp3⁺CD4⁺ regulatory T cells (**I**) determined. (**C** and **D**) Single-cell suspensions of tumor cells were stimulated with PMA and ionomycin, followed by intracellular cytokine staining for IFN-γ. Frequency of CD4⁺IFN-γ⁺ T cells (**C**) and CD8⁺IFN-γ⁺ T cells (**D**) was determined by flow cytometry. Data are representative of at least 3 independent experiments with $n \geq 3$ mice per experiment. (**E**) IFN-γ gene expression in WT and *Nlrc4*$^{-/-}$ tumors on day 12 after inoculation was determined by qPCR; data are pooled from 3 independent experiments with $n = 11$ WT and $n = 12$ *Nlrc4*$^{-/-}$ mice. Error bars represent SEM. (**A**–**I**) $^*P \leq 0.05$, $^{***}P \leq 0.001$, unpaired 2-tailed Student's *t* test.

AIM2 independent of inflammasome formation. Two recent studies highlight the role of AIM2, independent of the inflammasome, in suppression of colorectal cancer (45, 46). Man et al. showed that AIM2 played a role in suppressing aberrant proliferation of intestinal stem cells and controlling dysbiosis of the intestinal microbiota (45). Wilson et al. found AIM2 negatively regulated Akt activity, leading to decreased tumor burden (46). Both studies, along with our findings here, suggest that NLRC4 and AIM2 are able to modulate signaling pathways that are critical for controlling tumor growth independently of their roles in inflammasome activation.

The tumor-suppressing activity of NLRC4 was not limited to melanoma, but was also observed in a s.c. LLC tumor model. NLRC4⁺ tumor-associated macrophages were also detected in invasive melanoma from human patients. Evaluation of metastatic melanoma from human patients, suggesting advanced disease, revealed a surprising paucity of NLRC4⁺ tumor-associated macrophages compared with primary melanoma. It is unclear whether NLRC4 expression is suppressed or not induced in metastatic disease compared with primary invasive melanoma. Future studies will be required to directly answer these questions. However, the collective data presented here suggest that lower levels of NLRC4 are detrimental in controlling tumor growth. NLRC4 expression may also provide a useful biomarker to predict outcomes of patients with melanoma.

The protective role of NLRC4 in the B16F10 melanoma model was dependent in part on its expression within a hematopoietic cell that we hypothesize is most likely a macrophage,

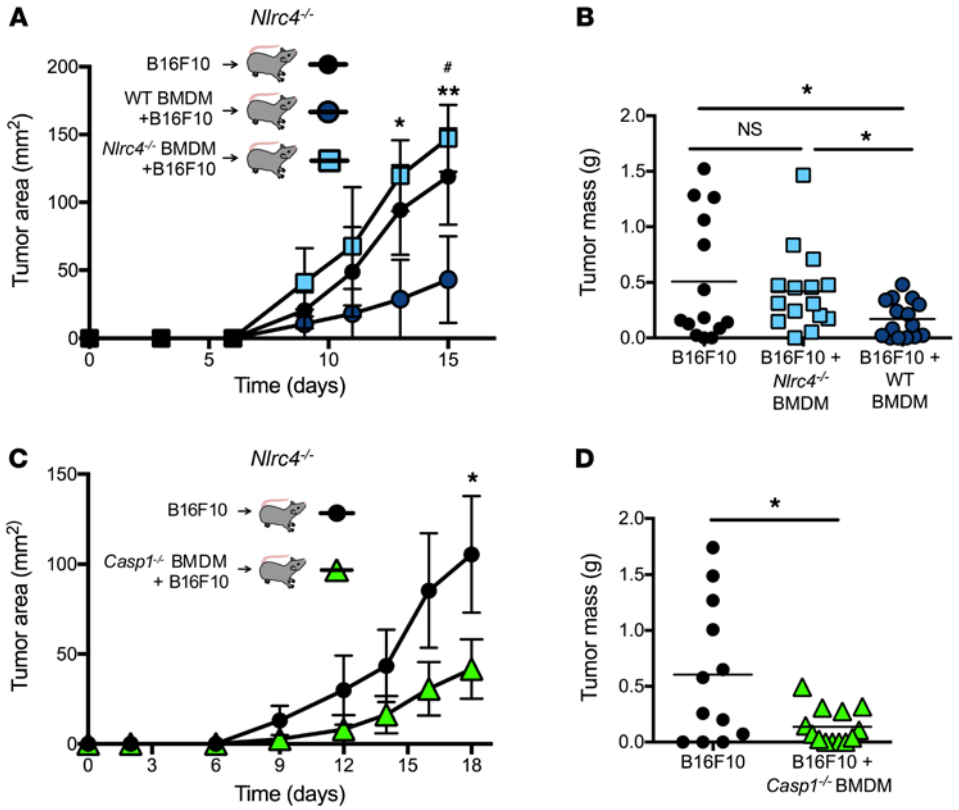

Figure 8. Expression of NLRC4, and not caspase-1, in macrophages regulates B16F10 tumor growth. (**A** and **B**) *Nlrc4*$^{-/-}$ mice were challenged s.c. with 1 × 10^5 B16F10 cells alone, a mixture of 1 × 10^5 B16F10 cells and 5 × 10^4 WT BMDMs, or 1 × 10^5 B16F10 cells and 5 × 10^4 *Nlrc4*$^{-/-}$ BMDMs. Tumor area was measured every 2 to 3 days (**A**). Tumor mass was determined at 15 days after inoculation (**B**). Data are representative of 2 experiments with n = 4 mice per group (**A**) or pooled from 3 independent experiments (n = 12–15 mice per group; **B**). (**C** and **D**) *Nlrc4*$^{-/-}$ mice were challenged s.c. with 1 × 10^5 B16F10 cells alone or a mixture of 1 × 10^5 B16F10 cells and 5 × 10^4 *Casp1*$^{-/-}$ BMDMs. Tumor area was measured every 2 to 3 days (**C**) and tumor mass was determined at 18 days after inoculation (**D**). Data are representative of 2 experiments each with n = 6 mice per group (**C**) or pooled from 2 independent experiments (n = 12–13 mice per group; **D**). (**A**) Error bars represent SEM. *$P \le 0.05$ and **$P \le 0.01$ (for B16F10 plus WT BMDMs compared with B16F10 plus *Nlrc4*$^{-/-}$ BMDMs); #$P \le 0.05$ (for B16F10 compared with B16F10 plus WT BMDMs), 2-way ANOVA with Tukey's HSD post-test for multiple comparisons. (**B** and **D**) *$P \le 0.05$, unpaired 2-tailed Student's t test. (**C**) Error bars represent SEM. *$P \le 0.05$, 2-way ANOVA with Sidak's multiple comparisons test.

as the delivery of WT, but not NLRC4-deficient, macrophages with tumor cells markedly inhibited tumor growth in *Nlrc4*$^{-/-}$ mice. This critical role for NLRC4 in macrophages was further supported by the defective cytokine and chemokine production by NLRC4-deficient macrophages, both isolated from tumors and stimulated in vitro. Evaluation of tumors from *Nlrc4*$^{-/-}$ mice revealed diminished STAT3 phosphorylation and increased p38 MAPK activation compared with tumors from WT mice. In the tumor microenvironment, TLRs are able to activate STAT3 signaling pathways, leading to subsequent inflammatory cytokine production (47–49). We have demonstrated that NLRC4-deficient macrophages have reduced production of proinflammatory cytokines in response to TLR stimulation. Hence, the decreased STAT3 phosphorylation in tumors from *Nlrc4*$^{-/-}$ mice may be due to defective TLR signaling.

Phosphorylation of p38α has been correlated with progression of a number of human cancers, including head and neck squamous cell carcinomas (50, 51). However, the mechanism by which NLRC4 regulates these signaling pathways and the relevance to tumor growth is still unknown. Interestingly, a number of NLR family members, including NLRP3, NLRP6, NLRP10, and NLRP12, have been implicated in regulating MAPK and NF-κB pathways (39–42, 52, 53). Therefore, our finding that NLRC4 can also affect these pathways is consistent with the broader function for NLR members in regulating immune responses.

We found the absence of NLRC4 is associated with a failure of CD4$^+$ and CD8$^+$ T cells to produce IFN-γ. This is an important finding, as immunotherapy for melanoma, in particular to augment the endogenous effector T cell response, has had promising clinical outcomes (54–58). Our data suggest that signaling through NLRC4 in macrophages helps to limit melanoma outgrowth and may subsequently promote T cell–mediated immunity. However, additional studies will be required to specifically determine whether the diminished chemokine production and reduced IFN-γ–producing CD4$^+$ and CD8$^+$ T cell populations directly influence tumor growth.

In summary, our study identifies an unconventional role for NLRC4 outside of bacterial recognition and inflammasome formation. We describe NLRC4 as an important regulator of key inflammatory signaling pathways in macrophages and demonstrate that the absence of NLRC4 leads to markedly enhanced tumor growth. Given the sterile nature of the tumor microenvironment, it is likely that NLRC4 is responding to an endogenous danger-associated molecular pattern, the identity of which will be

important to define. This may provide a therapeutic avenue that can be used to augment host immune responses against tumors.

Methods

Mice. C57BL/6N and B6-Ly5.2/Cr (CD45.1) mice were obtained from the National Cancer Institute mouse repository and Charles River Laboratories. The generation of *Nlrc4*$^{-/-}$, *Casp1*$^{-/-}$ (also deficient in *Casp11*), *Asc*$^{-/-}$, *Nlrp3*$^{-/-}$, *Nlrp6*$^{-/-}$, and *Nlrp12*$^{-/-}$ mice was previously described (59–63). All mice were backcrossed at least 10 generations onto a C57BL/6N background.

Cell lines. B16F10 melanoma cells (CRL-6332) and LLC cells (CRL-1642) were obtained from ATCC. Cell lines were cultured in DMEM supplemented with 10% heat-inactivated FCS, 2 mM L-glutamine, 100 U/ml penicillin G, and 100 μg/ml streptomycin.

Histology of human melanoma. Cases were selected randomly after approval by the Yale University Dermatopathology Tissue Committee, with the following criteria: tissue from greater than 5 years prior to this study, paraffin blocks containing ample material for study, and with respect to primary melanomas, tumors with a Breslow depth greater than 1 mm. All primary invasive and metastatic melanomas were clinically pigmented. Metastatic melanomas examined in this study were metastatic to skin. Tissues were stained with mouse anti-human CD163 (catalog MCA1853T, ABD Serotech) and rabbit anti-human IPAF (NLRC4) antibody (catalog 3107, ProSci). On each slide, the focus of greatest inflammation was identified, and 5 contiguous 20× high-power fields, each with an area of 3.14 mm^2, were quantified for CD163$^+$ or NLRC4$^+$ cells. The numbers of macrophages per case were normalized to unit area. For dual staining of primary melanomas, the EnVision G|2 Doublestain System (Dako) was used to stain CD163$^+$ cells with 3,3′-diaminobenzidine (brown) and NLRC4$^+$ cells with Permanent Red (red).

Tumor models. Female C57BL/6N WT or knockout mice were injected s.c. with either 1×10^5 B16F10 cells or 5×10^5 LLC cells. Tumor growth was measured every 2 to 3 days after tumor inoculation using digital calipers. Mice were sacrificed 15 to 20 days after inoculation and tumors excised and weighed to determine tumor mass. For qPCR and flow cytometry experiments, tumors were harvested 12 to 14 days after inoculation, when WT tumors became palpable.

For macrophage adoptive transfer experiments *Nlrc4*$^{-/-}$ mice were injected s.c. with 1×10^5 B16F10 cells alone or 1×10^5 B16F10 cells plus either 5×10^4 WT, *Nlrc4*$^{-/-}$, or *Casp1*$^{-/-}$ BMDMs. BMDMs were generated as previously described (64). Tumor growth and weight were determined as described above.

BM chimera. BM chimeras were generated as previously described (65). Briefly, CD45.1$^+$ WT or CD45.2$^+$ *Nlrc4*$^{-/-}$ mice were lethally irradiated with 500 Gy, followed by 450 Gy 4 hours later of whole-body irradiation. BM was harvested from donor CD45.1$^+$ WT or CD45.2$^+$ *Nlrc4*$^{-/-}$ femurs. Mice were reconstituted i.v. with 5×10^6 cells from donor BM. At least 5 weeks after BM transfer, mice were challenged with B16F10 cells s.c. as described above. Percentage of chimerism was determined by staining blood samples with anti-CD45.1 (clone A20; eBiosciences) and anti-CD45.2 (clone 104; eBioscience) antibodies for analysis by flow cytometry. Reconstitution was greater than 90% in *Nlrc4*$^{-/-}$ mice reconstituted with WT BM and 92% in WT mice reconstituted with *Nlrc4*$^{-/-}$ BM.

Ex vivo cell stimulations. Cells from the solid tumor or tumor-draining lymph node were incubated at 2×10^6 cells per well in a 96-well round-bottom plate (Corning). Cells were stimulated with 50 ng/ml PMA (Sigma-Aldrich) and 500 ng/ml ionomycin (Sigma-Aldrich) in the presence of 5 μg/ml brefeldin A (BioLegend) in RPMI 1640 complemented with 10% heat-inactivated FCS, 2 mM L-glutamine, 100 U/ml penicillin G, 100 μg/ml streptomycin, and 55 μM 2-ME (Gibco) for 6 hours at 37°C.

Flow cytometry. Single-cell suspensions of tumors were generated using a mouse tumor dissociation kit (Miltenyi Biotec) following the manufacturer's protocol. For extracellular staining, 2×10^6 cells were plated in a 96-well round-bottom plate (Corning). Cells were incubated first with Fixable Viability Dye eFluor 780 (eBioscience). Cells were incubated in the presence of CD16/CD32 (clone 93; eBioscience) to block Fc receptors and stained with combinations of antibodies for extracellular proteins: CD4 (clone GK1.5), CD8 (clone 53-6.7), CD45.1 (clone A20), CD45.2 (clone 104), CD90.2 (clone 53-2.1), CD11b (clone M1/70), CD11c (clone N418), F4/80 (clone BM8), Ly-6G (clone RB6-8C5) and MHCII (clone M5/114.15.2) (all antibodies obtained from eBioscience). Cells were stained in FACS buffer (PBS, 1% FCS, 1 mM EDTA, and 0.01% NaN_3) at 4°C for 30 minutes. Cells were then fixed with IC fixation buffer (eBioscience) for 20 minutes at room temperature. Samples were collected on a BD LSR II flow cytometer, and data were analyzed using FlowJo software (Tree Star).

For intracellular staining, cells were incubated with Foxp3/Transcription Factor Fixation/Permeabilization Buffer (eBioscience) overnight at 4°C to fix cells and then stained with anti–IFN-γ (clone XMG1.2; eBioscience) and anti-Foxp3 (clone FJK-16s; eBioscience) in Permeabilization Buffer for 30 minutes at room temperature. Cells were resuspended in FACS buffer and analyzed as described above.

To sort tumor cells, cells were stained with anti-CD45.2 (clone 104) and anti-F4/80 (clone BM8) as described above. Prior to cell sorting, Hoechst dye was added to samples to identify viable cells. Live cells were sorted using the BD Aria II and collected and pelleted for RNA isolation using the RNeasy Plus Micro Kit (QIAGEN) following the manufacturer's instructions.

Gene-expression analysis. For the RT^2 Mouse Cytokine and Chemokine PCR array (SA Bioscience), RNA was isolated from B16F10 tumors from C57BL/6N WT or *Nlrc4*$^{-/-}$ mice utilizing the RNeasy Fibrous Tissue Mini Kit (QIAGEN) following the manufacturer's protocol. cDNA was prepared from RNA using the SuperScript III Reverse Transcripatase Kit (Invitrogen) following the manufacturer's protocol. For qPCR array reactions, cDNA was mixed with RT^2 SYBR Green qPCR Mastermix (SA Bioscience), then aliquoted into the provided PCR plate containing primer pairs for various cytokines and chemokines. The array was run on a Mastercycer ep realplex (Eppendorf) following the PCR array protocol. qPCR array data were analyzed using the $2^{-\Delta Ct}$ method, where ΔCt = (Ct gene of interest – Ct housekeeping). Samples were normalized to the housekeeping genes *Actb*, *B2m*, *Gapdh*, *Gusb*, *Hsp90ab1*.

For all other qPCR reactions, RNA was isolated using either the RNeasy Fibrous Tissue Mini Kit (QIAGEN), the RNeasy Plus Mini Kit (QIAGEN), or the RNeasy Micro Kit (QIAGEN) following the manufacturer's instructions. cDNA was prepared from RNA as stated above. qPCR reactions were performed using cDNA, primer pairs for the indicated genes, and PerfeCta SYBR Green Fastmix (Quanta Biosciences). qPCR data were analyzed using the $2^{-\Delta Ct}$ method, where ΔCt = (Ct gene of interest – Ct housekeeping). For in vitro experiments where BMDMs were stimulated with B16F10 tumor homogenates, fold change in

gene expression was calculated using the $2^{-\Delta\Delta Ct}$ method, where ΔΔCt = [(Ct gene of interest - Ct housekeeping) stimulated – (Ct gene of interest – Ct housekeeping) unstimulated] (66). *Hprt* or *Actb* was used as a housekeeping gene.

Primer pairs for *Nlrc4*, *Hprt*, and *Actb* were obtained from QIAGEN. *Ifng*, *Cxcl9*, *Cxcl10*, *Cxcl13*, and *Cxcl16* primer pairs were all from Origene. Primer pairs for *Arg1*, *Fizz1*, and *Ym1* were obtained from Integrated DNA Technologies using previously described sequences (67).

In vitro stimulation of BMDMs. BMDMs were simulated with 50 ng/ml LPS, 50 μg/ml LTA, 100 ng/ml FSL-1, and 1 μg/ml Pam3CSK4 (Invivogen). After 20 hours, supernatants were collected and levels of IL-6 and IL-12p40 were determined via ELISA. Antibody pairs for ELISA were obtained from eBioscience. For chemokine gene expression analysis, BMDMs were stimulated for 9 hours with 100 μl of whole B16F10 tumors excised from WT mice and homogenized in PBS. Chemokine expression was determined via qPCR as stated above.

For immunoblot analysis BMDMs were stimulated with either 50 ng/ml LPS (Invivogen), 10 ng/ml recombinant murine IL-6 (PeproTech), 20 ng/ml TNF-α, 100 ng/ml TNF-α, or 10 g/ml anti-CD40 antibody for the indicated time points. Cells were lysed using RIPA buffer (Cell Signaling) supplemented with PMSF and used for immunoblotting.

Immunoblotting. Tumor lysates were prepared by homogenizing whole tumors in RIPA buffer (Cell Signaling) supplemented with PMSF using a Tissue-Tearor (BioSpec Products), and cell lysates were prepared as stated above. Tumor or cell lysates were separated on a NuPAGE gel followed by transfer to a PVDF membrane. Membranes were blocked in 5% nonfat milk and then incubated with primary antibody overnight at 4°C. Primary antibodies included the following: phospho-IκBα (catalog 2859), IκBα (catalog 4812), phospho-p38 MAPK (catalog 4511), p38 MAPK (catalog 8690), phospho-p44/42 MAPK (Erk1/2) (catalog 4370), p44/42 MAPK (Erk1/2) (catalog 4695), phospho-SAPK/JNK (catalog 4668), SAPK/JNK (catalog 9252), phospho-Stat3 (catalog 9131), Stat3 (catalog 9132), NF-κB2 p100/p52 (catalog 4882) (Cell Signaling), caspase-1 p20 (catalog AG-20B-0042-C100; Adipogen) and GAPDH (catalog CB1001; EMD Millipore). Following washing, membranes were then incubated with HRP-tagged secondary antibodies, anti-mouse IgG (1706516; Bio-Rad), or anti-rabbit IgG (NA934; GE Healthcare), and developed using SuperSignal West Femto or SuperSignal West Pico substrate (Thermo Fisher Scientific).

Statistics. Data were graphed using GraphPad Prism software. Statistical significance was determined either by unpaired 2-tailed Student's *t* test, 2-way ANOVA with Tukey's honest significant difference (HSD) or Sidak's post-test for multiple comparisons, or the Mann–Whitney *U* test. A *P* value of less than 0.05 was considered significant.

Study approval. All animal studies were approved by and performed according to the guidelines of the Institutional Animal Care and Use Committee at the University of Iowa. Use of human tissue in this study was approved by the Yale Human Investigation Committee, as part of the Yale Dermatopathology Stored Specimen Repository.

Author contributions

AMJ, SLC, and FSS conceptualized the project. AMJ, ORC, LAN, WZ, SLC, and FSS developed methodology. AMJ, EEH, and ORC performed experiments. AMJ, ORC, JMM, MDM, VPB, SLC, and FSS performed formal analysis. AMJ, SLC, and FSS wrote the original draft. AMJ, ORC, JMM, LAN, WZ, SLC, and FSS reviewed and edited the manuscript. SLC and FSS acquired funding. SLC and FSS supervised the project.

Acknowledgments

We thank Richard Flavell and Millennium Pharmaceuticals for providing knockout mice, Vickie Knepper-Adrian, Vincent Klump and Joyce Cheng for technical assistance, and Leslie Fox and Katie Fitzgerald at Iowa State University College of Veterinary Medicine Oncology Services for the care of Cookie Monster, the dog whose oral melanoma treatment played an instrumental role in the initiation of this work. NIH grants were as follows: R01 AI118719 (to FSS), R00 AI104706 (to SLC), T32 AI007485 (to AMJ), R01 CA158055 (to WZ), R01 CA200673 (to WZ). An American Cancer Society Seed Grant (to SLC), an Asthma and Allergy Foundation of America fellowship (to SLC), a Doris Duke Clinical Scientist Development Award 2015101 (to ORC), and a grant from the Harry J. Lloyd Charitable Trust (to FSS) supported this work. WZ was also supported by the V Scholar award, the Breast Cancer Research Award, and the Oberley Award (NCI Award P30CA086862) from the Holden Comprehensive Cancer Center at the University of Iowa.

Address correspondence to: Fayyaz Sutterwala, Cedars-Sinai Medical Center, 127 S. San Vicente Blvd., AHSP, Room A9106, Los Angeles, California 90048, USA. Phone: 310.423.2948; E-mail: Fayyaz.Sutterwala@cshs.org. Or to: Suzanne Cassel, Cedars-Sinai Medical Center, 8700 Beverly Blvd., South Tower, Room 6734, Los Angeles, California 90048, USA. Phone: 310.423.2584; E-mail: Suzanne.Cassel@cshs.org.

1. Siegel RL, Miller KD, Jemal A. Cancer statistics, 2016. *CA Cancer J Clin*. 2016;66(1):7–30.
2. Eggermont AM, Spatz A, Robert C. Cutaneous melanoma. *Lancet*. 2014;383(9919):816–827.
3. Grivennikov SI, Greten FR, Karin M. Immunity, inflammation, and cancer. *Cell*. 2010;140(6):883–899.
4. Lawrence MS, et al. Mutational heterogeneity in cancer and the search for new cancer-associated genes. *Nature*. 2013;499(7457):214–218.
5. Karachaliou N, et al. Melanoma: oncogenic drivers and the immune system. *Ann Transl Med*. 2015;3(18):265.
6. Krelin Y, et al. Interleukin-1beta-driven inflammation promotes the development and invasiveness of chemical carcinogen-induced tumors. *Cancer Res*. 2007;67(3):1062–1071.
7. Saijo Y, et al. Proinflammatory cytokine IL-1 beta promotes tumor growth of Lewis lung carcinoma by induction of angiogenic factors: in vivo analysis of tumor-stromal interaction. *J Immunol*. 2002;169(1):469–475.
8. Voronov E, et al. IL-1 is required for tumor invasiveness and angiogenesis. *Proc Natl Acad Sci U S A*. 2003;100(5):2645–2650.
9. Guo H, Callaway JB, Ting JP. Inflammasomes: mechanism of action, role in disease, and therapeutics. *Nat Med*. 2015;21(7):677–687.
10. Lamkanfi M, Dixit VM. Mechanisms and functions of inflammasomes. *Cell*. 2014;157(5):1013–1022.
11. Poyet JL, Srinivasula SM, Tnani M, Razmara M, Fernandes-Alnemri T, Alnemri ES. Identification of Ipaf, a human caspase-1-activating protein related to Apaf-1. *J Biol Chem*. 2001;276(30):28309–28313.
12. Zhao Y, Shao F. The NAIP-NLRC4 inflammasome in innate immune detection of bacterial flagellin and type III secretion apparatus. *Immunol Rev*. 2015;265(1):85–102.
13. Mariathasan S, et al. Differential activation of the inflammasome by caspase-1 adaptors ASC and Ipaf. *Nature*. 2004;430(6996):213–218.
14. Franchi L, Stoolman J, Kanneganti TD, Verma A, Ramphal R, Núñez G. Critical role for Ipaf in Pseudomonas aeruginosa-induced caspase-1 acti-

vation. *Eur J Immunol*. 2007;37(11):3030–3039.
15. Sutterwala FS, Mijares LA, Li L, Ogura Y, Kazmierczak BI, Flavell RA. Immune recognition of Pseudomonas aeruginosa mediated by the IPAF/NLRC4 inflammasome. *J Exp Med*. 2007;204(13):3235–3245.
16. Cai S, Batra S, Wakamatsu N, Pacher P, Jeyaseelan S. NLRC4 inflammasome-mediated production of IL-1β modulates mucosal immunity in the lung against gram-negative bacterial infection. *J Immunol*. 2012;188(11):5623–5635.
17. Amer A, et al. Regulation of Legionella phagosome maturation and infection through flagellin and host Ipaf. *J Biol Chem*. 2006;281(46):35217–35223.
18. Zamboni DS, et al. The Birc1e cytosolic pattern-recognition receptor contributes to the detection and control of Legionella pneumophila infection. *Nat Immunol*. 2006;7(3):318–325.
19. Lightfield KL, et al. Differential requirements for NAIP5 in activation of the NLRC4 inflammasome. *Infect Immun*. 2011;79(4):1606–1614.
20. Miao EA, et al. Cytoplasmic flagellin activates caspase-1 and secretion of interleukin 1beta via Ipaf. *Nat Immunol*. 2006;7(6):569–575.
21. Miao EA, et al. Innate immune detection of the type III secretion apparatus through the NLRC4 inflammasome. *Proc Natl Acad Sci U S A*. 2010;107(7):3076–3080.
22. Zhao Y, et al. The NLRC4 inflammasome receptors for bacterial flagellin and type III secretion apparatus. *Nature*. 2011;477(7366):596–600.
23. Franchi L, et al. Cytosolic flagellin requires Ipaf for activation of caspase-1 and interleukin 1beta in salmonella-infected macrophages. *Nat Immunol*. 2006;7(6):576–582.
24. Kofoed EM, Vance RE. Innate immune recognition of bacterial ligands by NAIPs determines inflammasome specificity. *Nature*. 2011;477(7366):592–595.
25. Rayamajhi M, Zak DE, Chavarria-Smith J, Vance RE, Miao EA. Cutting edge: Mouse NAIP1 detects the type III secretion system needle protein. *J Immunol*. 2013;191(8):3986–3989.
26. Yang J, Zhao Y, Shi J, Shao F. Human NAIP and mouse NAIP1 recognize bacterial type III secretion needle protein for inflammasome activation. *Proc Natl Acad Sci U S A*. 2013;110(35):14408–14413.
27. Hu B, et al. Inflammation-induced tumorigenesis in the colon is regulated by caspase-1 and NLRC4. *Proc Natl Acad Sci U S A*. 2010;107(50):21635–21640.
28. Nordlander S, Pott J, Maloy KJ. NLRC4 expression in intestinal epithelial cells mediates protection against an enteric pathogen. *Mucosal Immunol*. 2014;7(4):775–785.
29. Gajewski TF, Schreiber H, Fu YX. Innate and adaptive immune cells in the tumor microenvironment. *Nat Immunol*. 2013;14(10):1014–1022.
30. Kalluri R, Zeisberg M. Fibroblasts in cancer. *Nat Rev Cancer*. 2006;6(5):392–401.
31. Balkwill F. Cancer and the chemokine network. *Nat Rev Cancer*. 2004;4(7):540–550.
32. Kakinuma T, Hwang ST. Chemokines, chemokine receptors, and cancer metastasis. *J Leukoc Biol*. 2006;79(4):639–651.
33. Harlin H, et al. Chemokine expression in melanoma metastases associated with CD8+ T-cell recruitment. *Cancer Res*. 2009;69(7):3077–3085.
34. Mullins IM, et al. CXC chemokine receptor 3 expression by activated CD8+ T cells is associated with survival in melanoma patients with stage III disease. *Cancer Res*. 2004;64(21):7697–7701.
35. Walser TC, Ma X, Kundu N, Dorsey R, Goloubeva O, Fulton AM. Immune-mediated modulation of breast cancer growth and metastasis by the chemokine Mig (CXCL9) in a murine model. *J Immunother*. 2007;30(5):490–498.
36. Noy R, Pollard JW. Tumor-associated macrophages: from mechanisms to therapy. *Immunity*. 2014;41(1):49–61.
37. Biswas SK, et al. A distinct and unique transcriptional program expressed by tumor-associated macrophages (defective NF-kappaB and enhanced IRF-3/STAT1 activation). *Blood*. 2006;107(5):2112–2122.
38. Ostuni R, Natoli G. Transcriptional control of macrophage diversity and specialization. *Eur J Immunol*. 2011;41(9):2486–2490.
39. Allen IC, et al. NLRP12 suppresses colon inflammation and tumorigenesis through the negative regulation of noncanonical NF-κB signaling. *Immunity*. 2012;36(5):742–754.
40. Anand PK, et al. NLRP6 negatively regulates innate immunity and host defence against bacterial pathogens. *Nature*. 2012;488(7411):389–393.
41. Lich JD, et al. Monarch-1 suppresses non-canonical NF-kappaB activation and p52-dependent chemokine expression in monocytes. *J Immunol*. 2007;178(3):1256–1260.
42. Zaki MH, et al. The NOD-like receptor NLRP12 attenuates colon inflammation and tumorigenesis. *Cancer Cell*. 2011;20(5):649–660.
43. Yu H, Pardoll D, Jove R. STATs in cancer inflammation and immunity: a leading role for STAT3. *Nat Rev Cancer*. 2009;9(11):798–809.
44. Kaplan DH, et al. Demonstration of an interferon gamma-dependent tumor surveillance system in immunocompetent mice. *Proc Natl Acad Sci U S A*. 1998;95(13):7556–7561.
45. Man SM, et al. Critical Role for the DNA Sensor AIM2 in Stem Cell Proliferation and Cancer. *Cell*. 2015;162(1):45–58.
46. Wilson JE, et al. Inflammasome-independent role of AIM2 in suppressing colon tumorigenesis via DNA-PK and Akt. *Nat Med*. 2015;21(8):906–913.
47. Eyking A, et al. Toll-like receptor 4 variant D299G induces features of neoplastic progression in Caco-2 intestinal cells and is associated with advanced human colon cancer. *Gastroenterology*. 2011;141(6):2154–2165.
48. Herrmann A, et al. TLR9 is critical for glioma stem cell maintenance and targeting. *Cancer Res*. 2014;74(18):5218–5228.
49. Tye H, et al. STAT3-driven upregulation of TLR2 promotes gastric tumorigenesis independent of tumor inflammation. *Cancer Cell*. 2012;22(4):466–478.
50. Junttila MR, et al. p38alpha and p38delta mitogen-activated protein kinase isoforms regulate invasion and growth of head and neck squamous carcinoma cells. *Oncogene*. 2007;26(36):5267–5279.
51. Wagner EF, Nebreda AR. Signal integration by JNK and p38 MAPK pathways in cancer development. *Nat Rev Cancer*. 2009;9(8):537–549.
52. Lautz K, et al. NLRP10 enhances Shigella-induced pro-inflammatory responses. *Cell Microbiol*. 2012;14(10):1568–1583.
53. Wang L, et al. PYPAF7, a novel PYRIN-containing Apaf1-like protein that regulates activation of NF-kappa B and caspase-1-dependent cytokine processing. *J Biol Chem*. 2002;277(33):29874–29880.
54. Leach DR, Krummel MF, Allison JP. Enhancement of antitumor immunity by CTLA-4 blockade. *Science*. 1996;271(5256):1734–1736.
55. Freeman GJ, et al. Engagement of the PD-1 immunoinhibitory receptor by a novel B7 family member leads to negative regulation of lymphocyte activation. *J Exp Med*. 2000;192(7):1027–1034.
56. Topalian SL, et al. Safety, activity, and immune correlates of anti-PD-1 antibody in cancer. *N Engl J Med*. 2012;366(26):2443–2454.
57. Pardoll DM. The blockade of immune checkpoints in cancer immunotherapy. *Nat Rev Cancer*. 2012;12(4):252–264.
58. Hodi FS, et al. Improved survival with ipilimumab in patients with metastatic melanoma. *N Engl J Med*. 2010;363(8):711–723.
59. Arthur JC, et al. Cutting edge: NLRP12 controls dendritic and myeloid cell migration to affect contact hypersensitivity. *J Immunol*. 2010;185(8):4515–4519.
60. Elinav E, et al. NLRP6 inflammasome regulates colonic microbial ecology and risk for colitis. *Cell*. 2011;145(5):745–757.
61. Kuida K, et al. Altered cytokine export and apoptosis in mice deficient in interleukin-1 beta converting enzyme. *Science*. 1995;267(5206):2000–2003.
62. Lara-Tejero M, et al. Role of the caspase-1 inflammasome in Salmonella typhimurium pathogenesis. *J Exp Med*. 2006;203(6):1407–1412.
63. Sutterwala FS, et al. Critical role for NALP3/CIAS1/Cryopyrin in innate and adaptive immunity through its regulation of caspase-1. *Immunity*. 2006;24(3):317–327.
64. Sutterwala FS, Noel GJ, Clynes R, Mosser DM. Selective suppression of interleukin-12 induction after macrophage receptor ligation. *J Exp Med*. 1997;185(11):1977–1985.
65. Joly S, et al. Cutting edge: Nlrp10 is essential for protective antifungal adaptive immunity against Candida albicans. *J Immunol*. 2012;189(10):4713–4717.
66. Schmittgen TD, Livak KJ. Analyzing real-time PCR data by the comparative C(T) method. *Nat Protoc*. 2008;3(6):1101–1108.
67. Colegio OR, et al. Functional polarization of tumour-associated macrophages by tumour-derived lactic acid. *Nature*. 2014;513(7519):559–563.